Key Mechanistic Insights into the Intramolecular C-H Bond Amination and Double Bond Aziridination in Sulfamate Esters Catalyzed by Dirhodium Tetracarboxylate Complexes

Adrián Varela-Álvarez, Brandon E. Haines and Djamaladdin G. Musaev*

a) Cherry L. Emerson Center for Scientific Computation, Emory University, 30322 Atlanta, Georgia, USA.

E-mail: dmusaev@emory.edu (D.G.M.)

(Dedicated to Irina Petrovna Beletskaya)

ABSTRACT: Density Functional Theory was used to study the mechanisms of intramolecular C-H amination and olefin aziridination reactions of a variety of sulfamate esters. Particular emphasis is placed on the mechanism and factors governing amination of primary, secondary, tertiary and benzylic C-H bonds, the competition between tertiary and benzylic C-H amination, and the competition between allylic C-H amination and olefin aziridination. In these studies we used three different dirhodium paddlewheel catalysts, such as model $(H_2O)Rh_2(O_2CH)_4$ (**I**), $(H_2O)Rh_2(AcO)_4$ (**II**), and $(H_2O)Rh_2(esp)_2$ (**III**). In general, we found that all catalysts have a diamagnetic closed shell singlet state with a single Rh-Rh σ-bond. Active catalytic species in the studied amination reactions are triplet state dirhodium-nitrene complexes with the Rh–Rh single bond and Rh-N double bond (with one σ-bond and two "one-electron π-bonds"). From the active nitrenoid species, the C-H bond amination proceeds via triplet-to-singlet surface crossing and singlet state concerted C-H insertion mechanism. The calculated energy barriers correlate with the trend in homolytic bond dissociation energy of the activated C-H bonds. With the allylic substrate, the competing C=C double bond aziridination follows a stepwise pathway involving the formation of radical intermediate and radical coupling to produce singlet aziridination product. However, the allylic C-H bond amination occurs with a lower barrier which is consistent with experimental product distributions.

Keywords: C-H bond amination, Aziridination, Dirhodium-carboxylate catalyst, Density Functional approach, Selectivity

INTRODUCTION

Nitrogen-containing functional groups are ubiquitous in natural and pharmaceutical products, which makes C-N bond formation a main target in organic synthesis [1,2]. Direct C-H bond and an aliphatic C=C double bond functionalization through transition metal catalysis are appealing approaches to accomplish this important goal [3-6]. The use of C–H amination and C=C bond aziridination methods allow for direct access to the desired C–N functionality in a vast range of hydrocarbons and are cost-effective and environmentally friendly. Currently, there exist a number of examples of such processes utilizing various complexes of rhodium,[1-9] ruthenium,[1,2,10,11] cobalt,[2,12] iron,[2,13] copper,[2,14] and other metals.[2,15,16] Among these complexes, dirhodium paddlewheel complexes appear to be the most efficient. The structural motifs of dirhodium paddlewheel complexes and their stability during catalyst turnover allow selective functionalization of various C–H and C=C double bonds.[2,4-8,17] Indeed, a given substrate can possess different C–H centers and a competition between them during functionalization might arise. Common C–H bonds are terminal (primary), secondary, tertiary, and benzylic C-H bonds. It is expected that the degree of reactivity of these types of C–H bonds is different with tertiary and benzylic C-H bonds being the weakest based on homolytic bond dissociation energy. The positioning of an allylic C-H bond adjacent to a double bond imposes additional practical and mechanistic complexity because of competition between the C–H bond amination and double bond aziridination under essentially the same reaction conditions. Generally, such reactions result in undesirable mixtures of several products with low or no chemoselectivity and the product distribution is strongly catalyst- and substrate substrate-dependent.[18-21]

Thus, a deeper understanding of mechanisms and governing factors for selective amination of various C-H bonds, as well as C=C double bond in the presence of allylic C-H bond, is absolutely vital for designing selective transition metal catalysts for C-H and C=C bond amination. Therefore, one of goals of this paper is to elucidate the mechanisms and controlling factors for intramolecular amination of various (primary, secondary, tertiary, and benzylic, eq.1 in Scheme 1) C-H bonds in sulfamate esters catalyzed by dirhodium tetracarboxylates to generate oxathiazinanes, which was developed by Du Bois and co-workers.[19a,c-e,g-j,21] Another goal is to understand the mechanisms and controlling factors of selectivity between intramolecular C-H bond amination and C=C double bond aziridination for allylic substrates. For this purpose, we study these processes for olefin sulfamate esters catalyzed by dirhodium tetracarboxylate catalysts (Eq.2, in Scheme 1). In order to better understand reasons and impact of nature of dirhodium catalyst to selective tertiary and benzylic C-H amination we also study reaction (3) (see Scheme 1), which was previously reported. [11,19l]

In literature, several dirhodium catalysts were used to catalyze the targeted transformations. In earlier publications the simplest dirhodium tetracarboxylate $Rh_2(OAc)_4$ catalysts (see Scheme 2) has been widely employed.[19f,g,j] Later, the $Rh_2(esp)_2$ catalyst (where esp = □, □, □', □'–tetramethyl-1,3-benzenedipropanoate) as well as $Rh_2(OAc)_4$ catalyst [19e,h,j] is most extensively used.

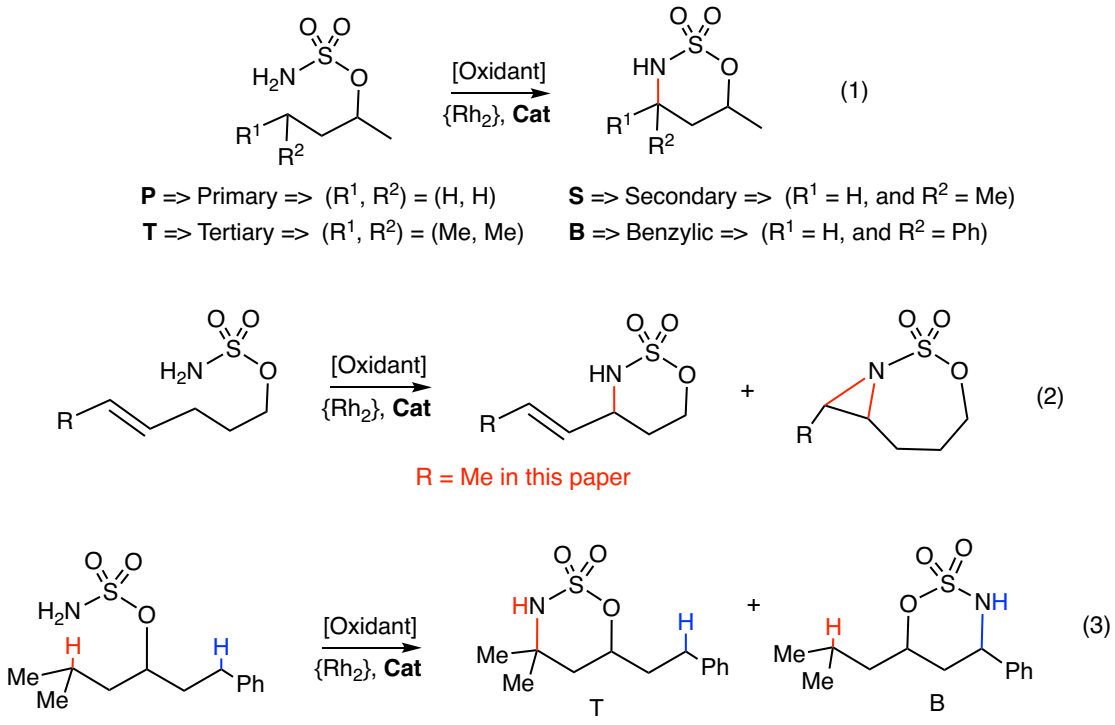

Scheme 1. Schematic presentation of various C–H bond amination in sulfamate ester (Eq.1), the allylic C–H bond amination and C=C double bond aziridination (Eq.2), and selective tertiary and benzylic C-H amination (Eq.3), catalyzed by different dirhodium catalysts. Selected reactions previously were reported by Du Bois and co-workers. [19f,g,j, 21]

Therefore, here, we use three different catalysts (Scheme 2): the experimentally relevant catalysts $(H_2O)Rh_2(OAc)_4$ and $(H_2O)Rh_2(esp)_2$, and the $(H_2O)Rh_2(O_2CH)_4$ model catalyst that is widely employed by theoreticians (see discussion below). We expect that comparison of the calculated data for real catalysts $(H_2O)Rh_2(OAc)_4$ and $(H_2O)Rh_2(esp)_2$, with those model catalyst $(H_2O)Rh_2(O_2CH)_4$ will allow us validate the applicability of the model extensively used in previous studies.

Scheme 2. Schematic representation of the used $(H_2O)Rh_2(O_2CH)_4$, $(H_2O)Rh_2(OAc)_4$ and $(H_2O)Rh_2(esp)_2$ catalysts in this study.

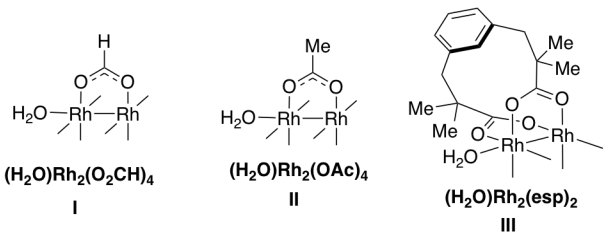

As mentioned above the reactions (1), (2) and (3) (see Scheme 1), previously were subject of several computational analyses. Zhao and co-workers [22] used the density functional approach and studied mechanism of the $Rh_2(O_2CH)_4$, Rh_2(*N*-methylformamide)$_4$ and Rh_2(*S*-nap)$_4$ catalyzed intramolecular benzylic C-H amination of 3-phenyl-propylsulfamate. The authors have shown that C–H amination starts from the Rh_2-nitrene intermediate with

lower-lying singlet and triplet electronic states. In general, singlet state process occurs via a concerted C-H insertion mechanism, while triplet state process may proceed via a stepwise pathway involving (a) intramolecular H-abstraction to generate a diradical intermediate, and (b) radical recombination to form final product. In a subsequent paper, Zhao and coworkers extended their study to elucidate the mechanism of the intramolecular allylic C–H amination and double bond aziridination in 4-pentenylsulfamate. [23] In this study, the authors used model catalysts $Rh_2(OAc)_4$, $Rh_2(NHCOCF_3)_4$ and $Rh_2(NCH_3CHO)_4$, and found: (a) the singlet concerted, highly asynchronous pathway for the C-H amination, and triplet stepwise pathway for the alkene aziridination reaction, and (b) the $Rh_2(OAc)_4$ and $Rh_2(CHCOCF_3)_4$ catalysts show similar reactivity patterns. In general, for all three catalysts, C-H amination is found to be more favorable than double bond aziridination.

Just recently, Wang and co-workers [24] have reported a comparative study of inter- and intramolecular (reaction 3, in Scheme 1) C–H amination by the $Rh_2(esp)_2$ catalyst. The authors have concluded that: (a) inter- and intra-molecular C–H bond amination proceed via different spin-state pathways, and the difference in the spin states is a reason for the observed benzylic-to-tertiary site selectivity switch; (b) the singlet- and triplet-state mechanisms are concerted hydride-transfer and stepwise H-atom abstraction processes, respectively, and (c) for the intramolecular C–H amination, the singlet-state concerted mechanism is dominant.

Thus, the previous computational studies on the reactions presented in Scheme 1 emphasize the utmost importance of investigating all three important reactions at the same level of theory and with the same model, as well as real, dirhodium tetracarboxylate catalysts. Furthermore, in the previously reported studies role of the axial water (or other coordinating molecules) ligand was mostly ignored. Therefore, our paper makes its goal to study these three reactions with the $(H_2O)Rh_2(O_2CH)_4$ model catalyst, and with the experimentally relevant $(H_2O)Rh_2(OAc)_4$ and $(H_2O)Rh_2(esp)_2$ catalysts. The discussion in this paper is organized as follows: At first, we briefly discuss geometry and electronic structures of all three catalysts and their nitrene complexes with saturated and unsaturated sulfamates. Then, we uncover intimate details of the reactions (1) and (2) catalyzed by model catalyst $(H_2O)Rh_2(O_2CH)_4$. Later, we elucidate catalyst impact to the mechanisms, and energy and geometry parameters of intermediates, transition states and products of the reactions (2) and (3). Lastly, we compare the results of the model catalyst to the experimentally relevant catalysts.

Calculation Procedures

Methods. In this paper, we used the M06L and M06 density functionals [25,26] in conjunction with the 6-31G(d,p) basis sets for C, H, N, O and S atoms [27] and LANL08(f) basis sets (with their corresponding ECPs) for Rh atoms (below called as basis sets BS1). [28] All reported structures were fully optimized without any geometry constraints. Previously, it was reported that the computational methods used in this paper accurately describe the energies and geometries of organometallic compounds. [11,29-33] Frequency calculations were carried out to verify the nature of the located stationary points. Graphical analysis of the imaginary vibrational normal modes, as well as the IRC calculations were used to confirm the nature of the located transition states.

Energetics of the reported structures were improved by performing single-point energy calculations at the M06L and M06 levels of theory in conjunction with the 6-311+G(df,p) basis sets for C, H, O, N, S atoms [27] and LANL08(f) for the Rh-centers (below called as basis sets BS2). In these calculations we used the M06L/BS1 and M06/BS1 optimized geometries, respectively. So, the final levels of methods used are M06L/BS2//M06L/BS1 and M06/BS2//M06/BS1. The reported thermodynamic data were computed at the 298.15K temperature and 1atm pressure. Solvent effects in dichloromethane were modeled by means of the PCM method. In these calculations, the free energy of solvation was computed as:

$$\square\square G_{solv} = G_{solv,PCM} - E_{el}$$

where the final free energy in solution is obtained as:

$$G_{solv} = G_{gas} + \square\square G_{solv}$$

All calculations were performed by the Gaussian_09 suite of programs. [34] NBO 3.1 program, which is included in Gaussian_09 suite of programs, was used to obtain natural bond orbitals (NBOs), atomic net charges, densities of spin and Wiberg bond indexes at the M06L/BS1 and M06/BS1 optimized geometries.

Our extensive analyses of the M06L and M06 calculated data and comparison of those with available experiments clearly demonstrates preference of the M06L functional over M06. Therefore, here we discuss only data obtained by the M06L density functional, i.e. by the M06L/BS2//M06L/BS1 method, while all energetics calculated at the M06 level are given in the Supporting Materials.

Below we use the following notations for the computed structures: ^{x}**Nm-y** for pre-reaction nitrene complexes, intermediates and products, and ^{x}**N-TSm-y** for transition states; where **X** = **P**(primary), **S**(secondary), **T**(tertiary), **B**(benzylic), **A**(aliphatic), **Al**(allylic) and **Az** (aziridination); **N** = **I** for $(H_2O)Rh_2(O_2CH)_4$, **II** for $(H_2O)Rh_2(AcO)_4$, and **III** for $(H_2O)Rh_2(esp)_2$; **m** = 0, 1, 2… for the order of the structure on the reaction coordinate; and **y** = **s** (singlet electronic state) and **t** (triplet electronic state).

RESULT AND DISCUSSION

(a) The (tetracarbooxylate)-bridged-Rh_2 catalysts $(H_2O)Rh_2(O_2CH)_4$, $(H_2O)Rh_2(AcO)_4$ and $(H_2O)Rh_2(esp)_2$: geometries and electronic structures. At first, we discuss the electronic structure and geometries of the dirhodium-tetracarboxylate complexes employed in this paper. Important structural parameters, the calculated atomic charges and spin densities of important atoms, as well as Wiberg indexes of vital bonds of these catalysts at their lowest singlet and triplet electronic states are collected on Figure 1 (for full geometries of these systems see Supporting materials). In Table 1, we present the calculated singlet-triplet energy splitting for these catalysts.

One should mention that the electronic structure of (tetracarboxylate)-Rh_2 complexes was previously discussed in detail. [8] Therefore, here we only briefly discuss electronic structure of complexes $(H_2O)Rh_2(O_2CH)_4$ (**I**), $(H_2O)Rh_2(AcO)_4$ (**II**), and $(H_2O)Rh_2(esp)_2$ (**III**).

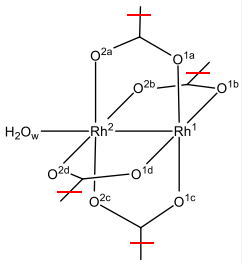

Distances (Wiberg Indexes)	$(H_2O)Rh_2(O_2CH)_4$, **I**		$(H_2O)Rh_2(AcO)_4$, **II**		$(H_2O)Rh_2(esp)_2$, **III**	
	Singlet	Triplet	Singlet	Triplet	Singlet	Triplet
$d(Rh^1\text{-}Rh^2)$	2.409 (0.83)	2.477 (0.55)	2.393 (0.82)	2.466 (0.54)	2.397 (0.82)	2.463 (0.54)
$d(Rh^1\text{-}O_w)$	2.305 (0.23)	2.542 (0.15)	2.335 (0.22)	2.595 (0.14)	2.326 (0.23)	2.591 (0.14)
$<d(Rh^1\text{-}O^{1x})>$	2.079 (0.42)	2.084 (0.41)	2.075 (0.43)	2.078 (0.42)	2.091 (0.41)	2.096 (0.40)
$<d(Rh^2\text{-}O^{2x})>$	2.079 (0.46)	2.099 (0.42)	2.075 (0.46)	2.093 (0.42)	2.089 (0.45)	2.111 (0.41)

Spin (Charge)	$(H_2O)Rh_2(O_2CH)_4$, **I**				$(H_2O)Rh_2(AcO)_4$, **II**				$(H_2O)Rh_2(esp)_2$, **III**			
	Singlet		Triplet		Singlet		Triplet		Singlet		Triplet	
	Mull.	NBO	Mull.	NBO	Mull.	NBO	Mull.	NBO	Mull.	NBO	Mull.	NBO
Rh^1	0.00 (0.76)	0.00 (0.65)	0.90 (0.76)	0.89 (0.68)	0.00 (0.75)	0.00 (0.65)	0.91 (0.76)	0.90 (0.69)	0.00 (0.69)	0.00 (0.65)	0.89 (0.69)	0.88 (0.68)
Rh^2	0.00 (0.75)	0.00 (0.59)	1.03 (0.77)	1.02 (0.68)	0.00 (0.72)	0.00 (0.59)	1.02 (0.75)	1.00 (0.68)	0.00 (0.73)	0.00 (0.61)	1.05 (0.76)	1.03 (0.71)
H_2O	0.00 (0.17)	0.00 (0.16)	0.04 (0.14)	0.05 (0.10)	0.00 (0.17)	0.00 (0.16)	0.04 (0.13)	0.04 (0.09)	0.00 (0.18)	0.00 (0.16)	0.04 (0.13)	0.05 (0.09)
$<S^2>$	0.00		2.01		0.00		2.01		0.00		2.02	

Figure 1. Schematic representation of the dirhodium-tetracarboxylate complexes, their calculated selected geometry parameters (in Å), spin densities and charges (in |e|) of their important atoms, as well as Wiberg indexes of vital bonds, at the lowest singlet and triplet electronic states of the catalysts.

For all studied catalysts, the diamagnetic closed shell singlet state is found to be the ground state. Frontier orbital and NBO analyses (see Figure S1) show that at their singlet states these complexes have an $[\sigma(d_{zz}+d_{zz})]^2[\pi(d_{xz}+d_{xz})]^2[\pi(d_{yz}+d_{yz})]^2[\delta(d_{xy}+d_{xy})]^2[\delta^*(d_{xy}-d_{xy})]^2[\pi^*(d_{xz}-d_{xz})]^2[\pi^*(d_{yz}-d_{yz})]^2[\sigma^*(d_{zz}-d_{zz})]^0$ electron configuration. Thus, the Rh-Rh bond in these complexes is formally a single bond and the Rh-centers are in their +2 oxidation states. These conclusions are in good agreement with the previous studies. [7,8, ,32,33,35,36]

The computed charge on the Rh-centers is largely independent of the nature of the bridging ligands and is in range of +0.69 – +0.76 |e| for catalysts **I**, **II** and **III**, respectively. The Rh-Rh atomic distances are also very close across these systems (2.409, 2.393 and 2.391 Å, respectively). The calculated value of Rh-Rh distance, 2.39–2.40 Å, is consistent with the single bond character of Rh–Rh bond. The calculated Wiberg bond indexes (WIs), which range from 0.82 to 0.83 also support this assignment. As it could be expected, the Rh^2–O_w bond distance is very sensitive to the catalyst considered (it ranges from 2.305 to 2.335 Å, see Figure 1). The calculated WIs for the Rh^2–O_w bond is 0.22 - 0.23.

The computed triplet states of these species are about 15-18 kcal/mol higher in energy. For these excited states, each Rh center has almost one unpaired spin regardless of the catalyst.

As usual, the Rh^1-center has slightly (ca 0.1 |e|) less unpaired spin than the water-coordinated Rh^2-center. The charge supported by the Rh_2-core is +0.69 – +0.76 |e|, which is same as that in singlet state. For all triplet state catalysts, the Rh-Rh bond has slightly larger than half-bond character according to the Wiberg bond indexes (0.54 – 0.55). Indeed, NBO analysis shows (see Figure S2) the existence of two beta Rh–Rh bonding orbitals. The first one is a Rh–Rh σ-bond (with population of 0.9 |e|), while the second one is a Rh–Rh π-bond (with population of 1.0 |e|). Thus, the Rh–Rh bond with half σ- and half π-bonds has more than half-bond character. Bearing in mind that one-electron σ-bond is intrinsically weaker than one-electron π-bond, one can explain slightly longer Rh–Rh bond distances in triplet states compared to their singlet states. Based on this discussion and electronic configuration of singlet states, one can assign the singlet-to-triplet transition in these catalysts as an electron transfer from the double occupied Rh–Rh π^*-orbital to unoccupied Rh–Rh σ^*-orbital (which is symmetry-allowed only under C_1-symmetry) Therefore, at their triplet state, these complexes have an $[\pi(d_{zz}+d_{zz})]^2[\pi(d_{xz}+d_{xz})]^2[\pi(d_{yz}+d_{yz})]^2[\sigma(d_{xy}+d_{xy})]^2[\pi^*(d_{xy}-d_{xy})]^2[\pi^*(d_{xz}-d_{xz})]^2[\pi^*(d_{yz}-d_{yz})]^1[\sigma^*(d_{zz}-d_{zz})]^1$ electron configuration.

Table 1. M06L/BS2//M06L/BS1 calculated relative electronic energies (ΔE), enthalpies (ΔH), free energies (ΔG) and free energies in CH_2Cl_2 (ΔG_{solv}) for the catalysts and active nitrene species. All values are given in kcal/mol.

Struct.	Mult.	$(H_2O)Rh_2(O_2CH)_4$, **I**				$(H_2O)Rh_2(AcO)_4$, **II**				$(H_2O)Rh_2(esp)_2$, **III**			
		ΔE	ΔH	ΔG	ΔG_{solv}	ΔE	ΔH	ΔG	ΔG_{solv}	ΔE	ΔH	ΔG	ΔG_{solv}
Cat.	s	0.0	0.0	0.0	0.0	0.0	0.0	0.0	0.0	0.0	0.0	0.0	0.0
	t	17.6	16.9	15.5	16.9	16.8	16.3	16.6	17.9	16.3	15.7	14.1	15.2
^{A}I0	t	-3.0	-4.2	-14.0	-10.3	-8.3	-9.5	-16.4	-13.2	13.6	-15.1	-24.0	-20.0
	s	2.6	1.2	-9.3	-6.2	-3.9	-2.7	-10.8	-7.8	-9.5	-10.9	-18.2	-14.6
^{P}I0	t	-1.1	-2.5	-13.3	-10.0	-	-	-	-	-	-	-	-
	s	3.6	2.1	-7.9	-4.9	-	-	-	-	-	-	-	-
^{S}I0	t	-1.7	-3.0	-13.3	-10.0	-	-	-	-	-	-	-	-
	s	3.2	1.6	-8.7	-5.7	-	-	-	-	-	-	-	-
^{T}I0	t	-2.9	-4.4	-15.0	-11.4	-7.7	-8.9	-17.0	-13.7	-13.3	-15.2	-24.8	-20.0
	s	1.9	0.5	-9.8	-6.6	-3.1	-4.6	-12.6	-9.8	-9.7	-11.3	-19.2	-14.6
^{B}I0	t	-3.5	-4.9	-14.5	-10.3	-10.0	-11.6	-20.1	-16.4	-15.8	-17.8	-26.4	-21.8
	s	1.5	-0.2	-10.3	-6.6	-5.5	-7.2	-14.9	-11.4	-11.5	-13.5	-21.7	-17.3

(b) Geometrical and Electronic properties of the reactive nitrenoids, **^{X}N0-y.** Next, we briefly analyze the electronic properties of the active nitrenoids **^{X}N0-y**. The electronic structures of these species also were subject of several previous studies. [7,8,11,22,23,24] Therefore, here we just briefly discuss our findings for the dirhodium-nitrene complex of the unsaturated sulfamate substrate, **^{A}N0-y** (for more information see Figure S3-S6 of Supporting materials). Our calculations show that these species may have several energetically close isomeric forms, which were labeled as **^{A}N0a-y** and **^{A}N0b-y**, respectively (see Figure 2).

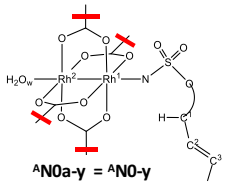

^{A}N0a-y = ^{A}N0-y

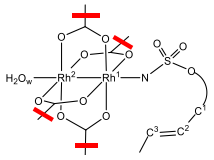

^{A}N0b-y

Distances (Wiberg Indexes)	$(H_2O)Rh_2(O_2CH)_4$, **I**		$(H_2O)(Rh_2(AcO)_4$, **II**		$(H_2O)Rh_2(esp)_2$, **III**	
	^{A}**I0-t**	^{A}**I0-s**	^{A}**II0-t**	^{A}**II0-s**	^{A}**III0-t**	^{A}**III0-s**
$d(Rh^1\text{-}Rh^2)$	2.432 (0.68)	2.452 (0.65)	2.415 (0.66)	2.430 (0.66)	2.419 (0.64)	2.439 (0.60)
$d(Rh^2\text{-}O_w)$	2.387 (0.20)	2.431 (0.18)	2.412 (0.19)	2.458 (0.17)	2.448 (0.18)	2.457 (0.18)
$d(Rh^1\text{-}N)$	1.981 (0.73)	1.960 (0.89)	1.976 (0.76)	1.966 (0.87)	1.972 (0.76)	1.975 (0.78)

Spin (Charge)	$(H_2O)Rh_2(O_2CH)_4$, **I**		$(H_2O)(Rh_2(AcO)_4$, **II**		$(H_2O)Rh_2(esp)_2$, **III**	
	^{A}**I0-t**	^{A}**I0-s**	^{A}**II0-t**	^{A}**II0-s**	^{A}**III0-t**	^{A}**III0-s**
Rh^1	0.40 (0.60)	-0.12 (0.61)	0.42 (0.63)	-0.13 (0.64)	0.40 (0.64)	-0.07 (0.63)
Rh^2	0.22 (0.58)	-0.46 (0.62)	0.28 (0.60)	-0.46 (0.64)	0.40 (0.65)	-0.58 (0.69)
N	1.18 (-0.56)	0.54 (-0.59)	1.06 (-0.58)	0.55 (-0.61)	1.01 (-0.61)	0.61 (-0.63)
$\langle S^2 \rangle$	2.02	0.62	2.02	0.62	2.02	1.01

Figure 2. Catalytic active nitrenoids relevant for the allylic C-H amination and C=C double bond aziridination. Some selected geometrical parameters (Å) and spin population values are included into these tables for different dirhodium complexes used in this paper.

For the sake of simplicity, here, we only discuss isomer ^{A}**N0a-y** (which will be called as ^{A}**N0-y**). We found that the triplet state nitrenoids, ^{A}**N0-t**, have nearly two unpaired spins (ranging from 1.76 |e| to 1.81 |e| □-spins) located on the Rh-Rh-N moiety (see Figure 2). However, these spins are delocalized slightly differently amongst the catalysts. The nitrenoid of $(H_2O)Rh_2(esp)_2$ exhibits the highest degree of radical delocalization (with 57-59% in N-center and 41-43% in Rh-Rh bond) among the three catalysts, while $(H_2O)Rh_2(O_2CH)_4$ exhibits the lowest delocalization (with 64-66% in N-center and 34-36% in Rh-Rh bond). Singlet state structures ^{A}**N0-s** of these nitrenoids are open-shell singlet states with about half a net □-electron on the nitrogen atom (0.5–0.6 |e|) and almost same amount of □-electron on the Rh_2-moiety.

As shown in Figure 2, for a given electronic state (for **y** = **s** or **t**) of the nitrenoid ^{A}**N0-y**, the longest Rh–Rh bond corresponds to the $(H_2O)Rh_2(O_2CH)_4$ catalyst (i.e. **N** = **I**) and the shortest one for the $(H_2O)Rh_2(esp)_2$-catalyst (i.e. **N** = **III**). Furthermore, for a given substrate and catalyst, the Rh–Rh bond is shorter for the triplet state nitrenoid ^{A}**N0-t**, than for the singlet ^{A}**N0-s**, while the Rh–N bond is shorter for ^{A}**N0-s** than ^{A}**N0-t**. In order to explain these trends, we analyzed the nature of the bonding in the triplet and singlet nitrenoid complexes. For the sake of simplicity, here we discuss only the nitrene complexes for catalyst **I** with the expectation that the major conclusions for this system will be valid for all other active species presented here. A set of selected NBO orbitals (those associated with Rh–Rh and Rh–N bonds, and N lone pairs) of these complexes are collected in Figures S3-S5 of the Supporting Information. NBO analysis shows no Rh–Rh bonding pattern in ^{A}**I0-s**. However, for ^{A}**I0-t** there are NBOs with □- and □*-bonding Rh–Rh character (with

populations of 0.66 |e| and 0.18 |e|, respectively). Thus, the Rh–Rh single bond, which was present in the catalyst is broken in the related nitrenoids although a trace of the Rh–Rh bond remains in the triplet state structure ^{A}**I0-t** (much less than half a single bond).

The difference of Rh–Rh bonding in ^{A}**I0-s** and ^{A}**I0-t** as discussed above correlates with the nature of the Rh–N bond in these species. Both ^{A}**I0-s** and ^{A}**I0-s** possess one alpha and one beta NBO associated with the Rh–N σ-bond (i.e. one full σ-bond). Obviously, nitrogen contribution to these orbitals is greater than Rh contribution and they can be considered something in between a covalent and an electrostatic interaction between N lone pair with the Rh(II) center. The singlet ^{A}**I0-s** Rh–N also has one π-bonding orbital and one nonbonding N orbital (see Figure S3), thus, ^{A}**I0-s** complex can be characterized with Rh=N double bond (with one σ- and one π-bonds) and N-lone pair.

In contrast, the triplet ^{A}**I0-t** has two nonbonding orbitals with one alpha spin each (instead of one double occupied nonbonding orbital in ^{A}**I0-s**), and two π-bonding orbitals with one beta spin each (instead of one double occupied π-bonding orbital in ^{A}**I0-s**) (see Figure S4). Thus, in triplet ^{A}**I0-t** the Rh–N bond has one σ-bond and two "one-electron π-bonds". As a result, the Rh–N bond is stronger in ^{A}**I0-s** than ^{A}**I0-t**. Strikingly, the triplet nitrenoids (for all considered catalysts and substrates) are more stable than their singlet analogues, which could be a consequence of increased Rh–Rh bonding.

The Rh–N binding energy in ^{A}**N0-s** and ^{A}**N0-t** (see Table 1) increases via **N** = **I** (10.0 - 11.4 kcal/mol) < **II** (13.1 – 16.4 kcal/mol) < **III** (20.0 – 21.8 kcal/mol) for given substrate (calculated from the ground states for all the active species). The singlet active species exhibit a similar but generally lower Rh-N formation free energy in solution: 6.6 – 4.9 kcal/mol for catalyst **I**, 11.4 – 7.8 kcal/mol for catalyst **II**, and 17.3 – 14.6 kcal/mol for catalyst **III**. Therefore, the most stable active species is always formed with catalyst **III** and the least stable is the one formed with catalyst **I**. These trends are consistent with the geometric and orbital analysis presented above, and are expected to have an impact on the computed reactivity and selectivity in the next section.

Dirhodium-nitrene complexes of the saturated sulfamate show similar bonding and electronic features, are presented in Supporting Materials (see Figures S7-S9) and will not be discussed here in details.

Comparison of the above presented data for $(H_2O)Rh_2$-nitrene intermediates of $(H_2O)Rh_2(O_2CH)_4$ (**I**), $(H_2O)Rh_2(AcO)_4$ (**II**) and $(H_2O)Rh_2(esp)_2$ (**III**) catalysts with those of $Rh_2(O_2CH)_4$, $(Rh_2(AcO)_4$, and $(Rh_2(esp)_2$, show that, in general, presence of axial water ligand has no significant impact on the calculated geometry, single-triplet splitting and electronic structures of the nitrenoid intermediates examined here.

(c) Mechanism of the reactions catalyzed by $(H_2O)Rh_2(O_2CH)_4$ model catalyst*: *C-H bond amination. Next, we discuss the mechanisms of the intramolecular C-H bond amination catalyzed by the model catalyst **I**. A schematic presentation of free energy reaction profiles of the reaction (1) for both singlet and triplet state species are shown in Table 2 along with their relative energies. The structures involved in these reactions, their complete energetics, geometry parameters, and NBO population data can be checked on Figure S8-S10 of Supporting Materials.

Table 2. Schematic presentation of energy profile of the C-H bond amination (Eq.1, in Scheme 1) catalyzed by catalyst **I**. The calculated relative energies of pre-reaction nitrene complexes, C-H activation transition states, intermediates and products are presented as □H(□G)[□G_{solv}] in kcal/mol.

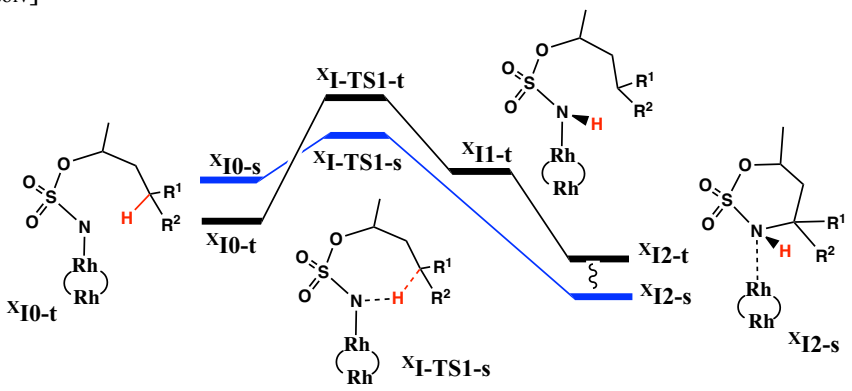

Structure	X = **P**	X = **S**	X = **T**	X = **B**
^{X}**I0-t**	0.0(0.0)[0.0]	0.0(0.0)[0.0]	0.0(0.0)[0.0]	0.0(0.0)[0.0]
^{X}**I0-s**	4.6(5.4)[5.1]	4.6(4.6)[4.3]	4.9(5.2)[4.8]	4.7(4.2)[3.7]
^{X}**I-TS1-t**	13.0(13.9)[13.5]	9.1(10.1)[9.5]	6.4(8.1)[7.8]	4.3(5.2)[4.3]
^{X}**I-TS1-s**	11.1(13.2)[11.5]	6.1(8.5)[7.1]	4.5(7.4)[6.5]	2.9(5.0)[3.4]
^{X}**I1-t**	7.6(6.9)[6.6]	3.0(2.5)[1.7]	-0.8(-0.9)[-1.7]	-8.5(-7.5)[-8.6]
^{X}**I1-s**	----	----	----	----
^{X}**I2-t**	-32.4(-33.1)[-33.2]	-34.6(-35.3)[-35.0]	-34.8(-34.5)[-33.8]	-32.9(-33.0)[-33.2]
^{X}**I2-s**	-54.6(-52.0)[-51.8]	-56.9(-54.0)[-53.7]	-56.4(-53.5)[-52.8]	-54.6(-52.2)[-52.1]

A quick look at the reaction profile and associated energetics (Table 2) reveals that the singlet and triplet states of the structures involved in the C-H bond amination are very close in energy, and the triplet and singlet energy surfaces are likely to cross (see also, [22-24]). Similar two-state reactivity was previously reported by us for the $[Ru_2Cl(hp)_4]^+$ catalyzed C-H aminations. [11] Here, we did not locate this triplet-singlet crossing points, but it is evident that this occurs *before* the C-H activation transition state. [37]

As shown in Table 2, for all the substrates studied here, the ground electronic states of active species (i.e., nitrenoids) are triplet states (^{X}**I0-t**) while those for products are the singlet states (^{X}**I2-s**). For the C–H activation transition states ^{X}**I-TS1-y**, the ground electronic states are singlet states (**y** = **s**). Thus, the reaction is initiated from the triplet state pre-reaction complex ^{X}**I0-t** and proceeds via the triplet-singlet surface crossing and singlet C-H activation transition state ^{X}**I-TS1-s** to form the singlet state products ^{X}**I2-s**.

Close examination of the singlet transition state structure ^{X}**I-TS1-s** shows that it can be characterized as a concerted C-H insertion transition state, where hydrogen abstraction and C-N bond formation take place simultaneously (see Supporting Materials). As mentioned above, the triplet nitrenoids have a relatively weak Rh-Rh bond (with WI = 0.67 – 0.68) and a strong Rh^1-N bond (with WI = 0.73 – 0.75). On the other hand, the product complexes ^{X}**I2-s** have a strong Rh-Rh bond (with WI = 0.80 – 0.81) indicating that

breaking the Rh^1-N bond facilitates recovery of the Rh-Rh single bond of the active catalyst. As expected, the transition-state structures exhibit geometrical features that are in between those for the pre-reaction (**^{X}I0-t**) and product (**^{X}I2-s**). For instance, for the activated C-H bond the WI is calculated to be within 0.28 - 0.61, while it is in a range of 0.24 – 0.55 for the nascent N-H bond (d_{NH} = 1.147 - 1.501 Å).

Comparison of the C–H activation barriers (calculated as the energy difference between pre-reaction complex **^{X}I0-t** and corresponding transition state **^{X}I-TS1-s**) shows that they decrease via the trend: primary (11.5 kcal/mol) > secondary (7.1 kcal/mol) > tertiary (6.5 kcal/mol) > benzylic (3.4 kcal/mol). This trend is consistent with the observed trend in homolytic bond dissociation energy of the activated C-H bonds: [primary (CH_3CH_3 → $CH_3CH_2^{\cdot}$ + $H^{\cdot}$, 101.1 ± 0.4 kcal/mol)] > [secondary ($CH_3CH_2CH_3$ → $CH_3CH^{\cdot}CH_3$ + $H^{\cdot}$, 98.6 ± 0.4 kcal/mol)] > [tertiary ($(CH_3)_3CH$ → $(CH_3)_3C^{\cdot}$ + $H^{\cdot}$, 96.5 ± 0.4 kcal/mol)] > [benzylic (PhCH3 → $PhCH_2^{\cdot}$ + $H^{\cdot}$, 89.8 ± 0.6 kcal/mol)].[38]

The C–H activation barriers for the triplet state, **^{X}I-TS1-t**, are higher but follow the same trend based on the substrate as the singlet transition states (see Table 2). The triplet state transition states can be characterized as a hydrogen abstraction transition state leading to radical intermediate **^{X}I1-t** (see Supporting Materials). Along the triplet state reaction coordinate, the spin population of the Rh-Rh-N fragments of pre-reaction complex **^{X}I0-t** decreases from ~ 2 |e| to ~ 1 |e|: 1.80 |e| for **^{X}I0-t** □ (1.33 – 1.39 |e|) for **^{X}I-TS1-t** □ (0.85 – 1.00 |e|) for **^{X}I1-t** (see Supporting materials). On the other hand, the spin population of the generated radical centers (C^1 atom, or C^1Ph, or C^1-C^2-C^3 groups) increases from ~ 0 |e| to ~ 1 alpha |e|: (0.00 – 0.02 |e|) for **^{X}I0-t** □ (0.44 – 0.54 |e|) for **^{X}I-S1-t** □ (0.89 – 1.00 |e|) for **^{X}I1-t**. Radical coupling in **^{X}I1-t** completes the C-N bond formation with a six-membered ring final product. (We were not able to locate this ring-closure transition state, which is expected to occur with small energy barrier associated with alpha-to-beta spin-flip).

In summary, from the presented analysis we conclude that the primary (X=P), secondary (X=S), tertiary (X=T) and benzylic (X=B) C–H amination proceeds via the concerted C-H insertion mechanism. Furthermore, the calculated energy barriers correlate with the observed trend in homolytic bond dissociation energy of the activated C-H bonds.

The above presented mechanistic conclusion for benzylic C–H amination by catalyst $(H_2O)Rh_2(O_2CH)_4$ (**I**) is in excellent agreement with that previously reported [22] for catalyst $Rh_2(O_2CH)_4$

(d) Mechanism of the reactions catalyzed by model catalyst*: *allylic C-H bond amination vs C=C double bond aziridination. As mentioned above, for the sulfamates that contain an allylic C-H bond, the C-H bond amination can compete with aziridination of the double bond (Eq.2). Here we present our computational findings for the $Rh_2(H_2O)(O_2CH)_4$ catalyzed intramolecular allylic C-H bond amination and double bond aziridination in the same substrate. The free energy reaction profiles of these processes (schematically) and relative energies of reactants, transition states, intermediates and products are presented in Table 3. The structures involved in these reactions, their complete energetics, geometry parameters, and NBO population data can be checked on Figure S11-S13 of the Supporting Information.

Table 3. Schematic presentation of energy profile for competing allylic C-H amination and C=C double bond aziridination in unsaturated sulfamate studied in this paper, and calculated relative energies (presented as □H(□G)[□G_{solv}] and given in kcal/mol) of pre-reaction nitrene complexes, transition states, intermediates and products for catalyst **I**.

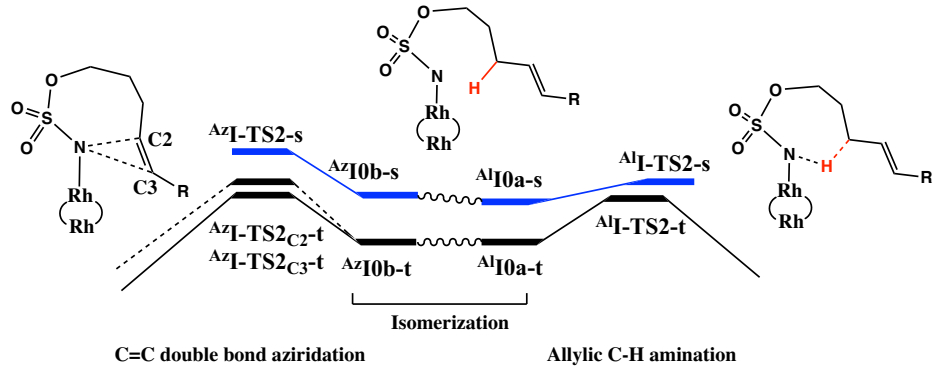

Structure	X = **Al**	**X = Az**	
	Z = none	**Z = C2**	**Z = C3**
^{X}**I0a-t**	0.0(0.0)[0.0]	0.0(0.0)[0.0]	0.0(0.0)[0.0]
^{X}**I0a-s**	5.4(4.7)[4.1]	-----	-----
^{X}**I0b-t**	-----	-1.7(-0.3)[-0.5]	-----
^{X}**I0b-s**	-----	3.3(5.1)[4.5]	-----
^{X}**I-TS2$_{Z}$-t**	3.5(5.6)[4.3]	5.0(7.6)[7.7]	4.5(6.7)[7.4]
^{X}**I-TS2-s**	3.4(6.5)[4.5]	7.5(10.3)[9.8]	7.5(10.3)[9.8]
^{X}**I3$_{Z}$-t**	-12.5(-11.5)[-12.4]	-9.0(-6.5)[-5.5]	-10.0(-8.1)[-6.8]
^{X}**I3-s**	-----	-----	-----
^{X}**I4-t**	-34.7(-33.5)[-32.6]	-25.8(-23.6)[-21.5]	-25.8(-23.6)[-21.5]
^{X}**I4-s**	-55.8(-53.6)[-52.6]	-44.9(-40.5)[-38.6]	-44.9(-40.5)[-38.6]

Similar to the intramolecular C-H bond amination discussed above, intramolecular allylic C-H amination and double bond aziridation (see reaction 2) starts from the triplet state pre-reaction complex ^{A}**I0a-t** and ^{A}**I0b-t**, respectively, but leads to the singlet state amination and aziridine products ^{Al}**I4-s** and ^{Az}**I4-s**, respectively (see Table 3). Thus, the triplet and singlet spin states are crossing again, and two-state reactivity is becoming a general feature of this catalyst. For these reactions, we located several transition states on the singlet and triplet PES, including two regioisomeric transition states on the triplet PES (^{Az}**I-TS2$_{C2}$-t** and ^{Az}**I-TS2$_{C3}$-t**). As shown in Table 3, transition state ^{Az}**I-TS2-s** is energetically higher than its triplet state analogues (see Supporting materials for more details). This indicates that reaction proceeds via the triplet transition states (^{Az}**I-TS2$_{C2}$-t** and ^{Az}**I-TS2$_{C3}$-t**) and the singlet-triplet surface crossing occurs somewhere *after* the rate-limiting transition state

structures. Therefore, this singlet-triplet surface crossing is not going impact to our overall conclusions and will not be discussed further.

Briefly, analyses of the geometry, spin density and bond order along the energetically lowest triplet reaction coordinate (see Supporting Materials for more details) suggest stepwise aziridine formation through an initial radical addition to the olefin to form a diradical intermediate and subsequent radical coupling mechanism to cleave the Rh^1-N bond and regenerate the Rh-Rh single bond of the active catalyst. The triplet transition states **^{Az}I-TS2$_{C2}$-t** and **^{Az}I-TS2$_{C3}$-t** connect pre-reaction complex **^{Az}I0b-t** with the seven-membered and eight-membered ring intermediates **^{Az}I3$_{C2}$-t** and **^{Az}I3$_{C3}$-t**, respectively. The difference between these two pathways stems from which N-C bond is formed first, either the N-C2 bond or the N-C3 bonds, respectively. Calculations show that solvation free energy barriers at the **^{Az}I-TS2$_{C2}$-t** and **^{Az}I-TS2$_{C3}$-t** are 7.7 and 7.4 kcal/mol calculated relative to the **^{Az}I0-t** pre-reaction complex, respectively. However, both pathways lead to the same final aziridine product **^{Az}I4-t**.

Bearing in mind that the lowest allylic amination barrier is 4.3 kcal/mol (at transition state **^{Al}I-TS2-t**) and that the lowest aziridination barrier is 7.9 kcal/mol, one can conclude that intramolecular allylic C-H amination is preferred over double bond aziridination for sulfamates where both are possible if catalyst **I** is used. This result (i.e. trend) is qualitatively consistent with the available experimental data employing catalyst **II**, $(H_2O)Rh_2(AcO)_4$, which produces a 2:1 amination:aziridination product ratio. [19f,g,j]

(e) From the model to reality: catalyst effect on the tertiary vs. benzylic C-H amination. In order to validate the conclusions made above for the model catalyst **I**, we also studied tertiary and benzylic C-H amination in equation (3) by the experimentally relevant catalysts **II** and **III**, i.e. $(H_2O)Rh_2(OAc)_4$ and $(H_2O)Rh_2(esp)_2$, respectively. For the sake of simplicity, here we discuss only the effect of the nature of the catalyst on the most important structures of the reaction, namely, the active nitrenoid and the C-H activation transition states. Comparison of the potential energy surfaces of the tertiary and benzylic C-H amination for the different catalysts are shown in Figure 3. The geometrical parameters, NBO spin populations and detailed energetic values of the main structures involved are collected in figure S14 of Supporting materials.

Like in model catalyst **I**, the nitrenoids of catalysts **II** and **III** also have the triplet ground states. Again, for all the six combinations of the three catalysts and two substrates (tertiary and benzylic), the singlet transition state structure **^{X}N-TS1-s** is lower in energy than the corresponding triplet state structures. *Thus, for all three catalysts the tertiary and benzylic C-H activation proceeds via the concerted mechanism.* The experimental test with non-allylic substrates previously reported by Du Bois and co-workers indicates that a concerted mechanism is more likely than a stepwise, which is in full agreement with our predictions. [11,19g,19j] This finding, once again, confirms applicability of $(H_2O)Rh_2(O_2CH)_4$ as a model to probe the electronic structure and reactivity of experimental catalysts $(H_2O)Rh_2(OAc)_4$ and $(H_2O)Rh_2(esp)_2$. Also, we should indicate that our findings for the $(H_2O)Rh_2(esp)_2$ catalyst are consistent with those recently reported by Wang and co-workers [24].

Comparison of the calculated solvation free energy barriers (calculated relative to the triplet state of active nitrene species) shows that they are 6.5, 6.4 and 5.6 kcal/mol for the tertiary C-H bond, and 3.4, 8.1 and 8.2 kcal/mol for the benzylic C-H bond, for catalysts **I**, **II** and **III**, respectively. Analyses of the energetically lowest singlet state barriers show that the ratio of tertiary:benzylic amination is affected by the nature of catalyst. Indeed, for model catalyst **I** calculations favor benzylic C-H amination by 3.1 kcal/mol, which is inconsistent with the available experiments. However, for catalysts **II** and **III** our calculations favor the tertiary C-H amination by 1.7 and 2.6 kcal/mol, respectively. These findings are in reasonable agreement with the available experiments showing 1.5:1 and 7:1 tertiary:benzylic ratio for catalysts **II** and **III**, respectively. These findings suggest that the $(H_2O)Rh_2(O_2CH)_4$ catalyst is not an adequate model for predicting the selectivity of experimental catalysts, such as $(H_2O)Rh_2(OAc)_4$ and $(H_2O)Rh_2(esp)_2$. Thus, one should be careful about choosing a model based on the properties of interest.

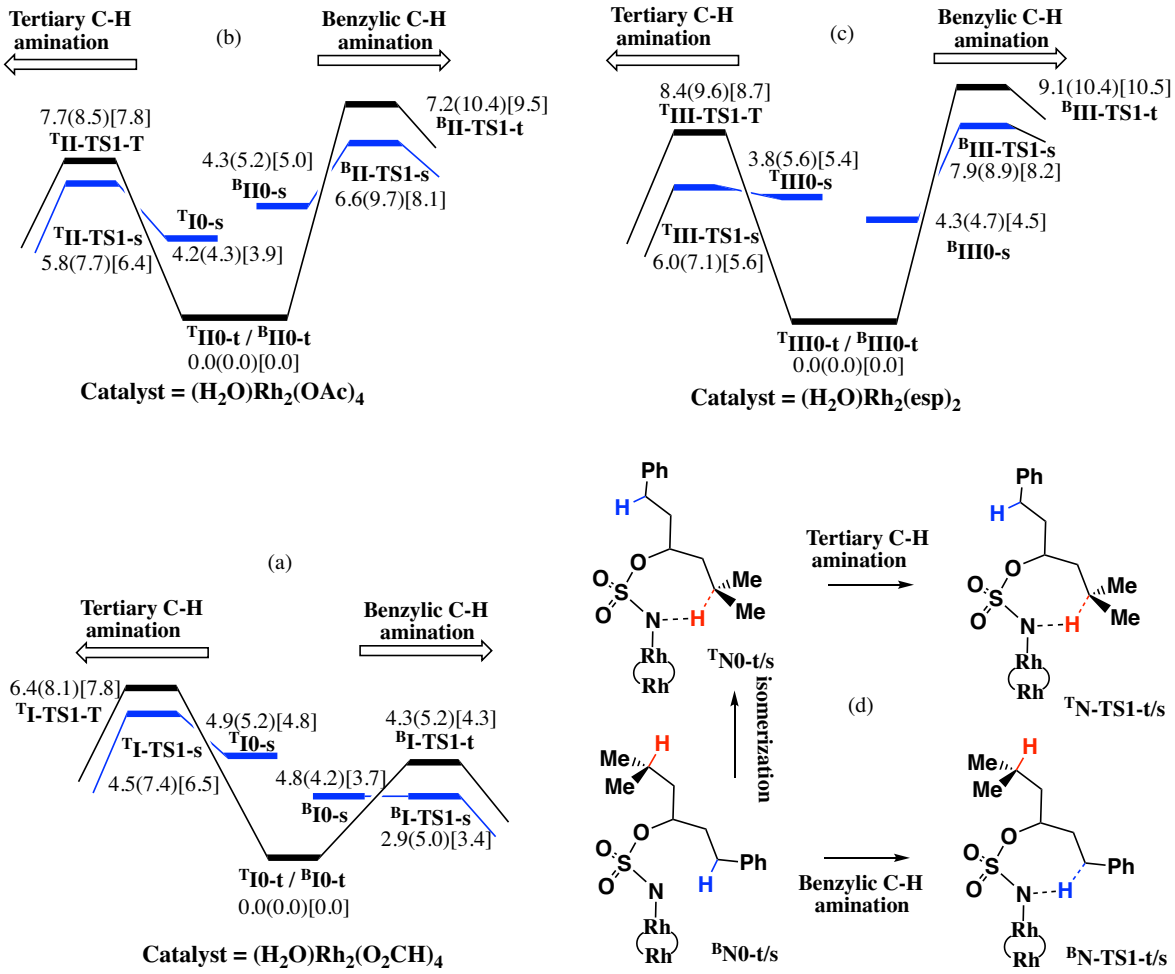

Figure 3. Calculated energy profiles (scaled to in solution free energies) for the tertiary and benzylic C-H amination catalyzed by the three different catalysts (a-c) studied in this paper, and (d) schematic presentation of the corresponding pre-reaction complexes and transition states. All energies given as $\Delta H(\Delta G)[\Delta G_{solv}]$ are in kcal/mol.

In order to further validate our conclusion, we performed KIE calculations for this reaction (see Table 4). Agreement with the available experiment is better for the transition state on the singlet surface than the triplet surface, which is consistent with concerted C-H insertion mechanism of the reaction. The origin of the errors in the calculated KIEs, most likely, arises from the true nature of the calculated transition state structures, which do not incorporate the spin-flip effect (see also [39]).

Table 4. Kinetic Isotopic Effects (KIEs) computed at the M06L/BS1 level of theory

Catalyst	$(H_2O)Rh_2(O_2CH)_4$	$(H_2O)Rh_2(OAc)_4$		$(H_2O)Rh_2(esp)_2$
TS1-s	3.4	4.5	2.6	5.0
TS1-t	5.7	5.7	(Exp. Value)[11]	5.7

(f) From the model to reality: catalyst effect on the allylic C-H amination vs. double bond aziridination. We also elucidated the impact of the nature of the catalyst on the mechanisms and competition between allylic amination and aziridination. In particular we studied the amination:aziridination ratio. In Table 5 we show the reaction profiles of the allylic C-H amination and double bond aziridination for catalysts **I**, **II** and **III**. In Figure S15 we show selected geometrical parameters and Mulliken spin populations for the most important structures of the reactions for each catalyst.

Table 5. Schematic presentation of energy profile of the allylic C-H amination and C=C double bond aziridination in unsaturated sulfamate studied in this paper, and calculated relative energies (presented as □H(□G)[□G_{solv}] and given in kcal/mol) of pre-reaction nitrene complexes, transition states, intermediates and products for catalysts **I** (presented here again to make easier to compare results), **II** and **III**.

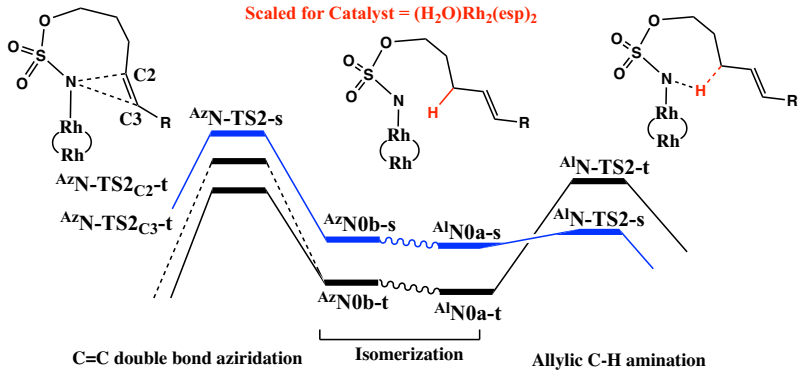

Structure	X = **Al**	**X = Az**	
	Z = NONE	**Z = C2**	**Z = C3**
	Catalyst = $(H_2O)Rh_2(O_2CH)_4$, I		
^{X}I0a-t	0.0(0.0)[0.0]	0.0(0.0)[0.0]	0.0(0.0)[0.0]
^{X}I0a-s	5.4(4.7)[4.1]	-----	-----
^{X}I0b-t	-----	-1.7(-0.3)[-0.5]	-----
^{X}I0b-s	-----	3.3(5.1)[4.5]	-----

^{X}I-TS2$_{Z}$-t	3.5(5.6)[4.3]	5.0(7.6)[7.7]	4.5(6.7)[7.4]
^{X}I-TS2-s	3.4(6.5)[4.5]	7.5(10.3)[9.8]	7.5(10.3)[9.8]
	Catalyst = $(H_2O)Rh_2(OAc)_4$, II		
^{X}II0a-t	0.0(0.0)[0.0]	0.0(0.0)[0.0]	0.0(0.0)[0.0]
^{X}II0a-s	4.1(4.3)[4.0]	-----	-----
^{X}II0b-t	-----	-0.6(0.3)[0.2]	-----
^{X}II0b-s	-----	4.0(4.4)[3.9]	-----
^{X}II-TS2$_{Z}$-t	5.3(6.8)[5.7]	7.3(9.0)[9.4]	7.4(8.3)[9.1]
^{X}II-TS2-s	5.9(9.4)[7.5]	11.2(13.0)[12.8]	11.2(13.0)[12.8]
	Catalyst = $(H_2O)Rh_2(esp)_2$, III		
^{X}III0a-t	0.0(0.0)[0.0]	0.0(0.0)[0.0]	0.0(0.0)[0.0]
^{X}III0a-s	4.2(5.8)[5.4]	-----	-----
^{X}III0b-t	-----	-0.1(0.4)[1.5]	-----
^{X}III0b-s	-----	4.2(6.3)[7.6]	-----
^{X}III-TS2$_{Z}$-t	8.7(10.8)[10.5]	7.8(10.2)[11.3]	4.9(8.1)[9.1]
^{X}III-TS2-s	7.1(9.1)[7.6]	10.4(14.0)[14.4]	10.4(14.0)[14.4]

Again, regardless of the catalyst used, the triplet states are the ground states for the catalytic active nitrenoids **^{A}N0** and **^{Az}N0**. The triplet allylic amination transition states are lower than the singlet states for catalysts **I** and **II**. However, for catalyst **III** the singlet state of the allylic amination transition state is 2.9 kcal/mol lower than the triplet state. Thus, while for catalysts **I** and **II**, both the concerted and stepwise mechanisms are viable for the allylic C-H amination, but for catalyst **III** the concerted mechanism becomes more preferable. Furthermore, data presented in Table 5 show that the allylic C-H amination reactivity of these catalyst changes via **N = I** [4.3 kcal/mol] < **II** [5.7 kcal/mol] < **III** [7.6 kcal/mol].

For the aziridination reaction, both triplet transition states, **^{Az}N-TS2$_{C2}$-t** and **^{Az}N-TS2$_{C3}$-t**, are lower in energy than the singlet one, regardless of the catalyst employed. The solution free energy gap between two lowest triplet transition state structure **^{Az}N-TS2$_{C2}$-t** and **^{Az}N-TS2$_{C3}$-t** is 0.3 kcal/mol for catalyst **I** and **II**, but increases to 2.2 kcal/mol for catalyst **III**. Computed from **^{Az}N0-t**, the free energies in solution of triplet transition state for the double bond aziridination are **N=I** [7.4 kcal/mol] < **II** [9.1 kcal/mol] = **III** [9.1 kcal/mol].

Comparison of above presented data for allylic C-H amination and double bond aziridination by three different catalysts show that all utilized catalysts favor allylic C-H amination over double bond aziridination (by 3.1, 3.4 and 1.5 kcal/mol for catalysts **I**, **II** and **III**, respectively). This finding is in good qualitative agreement with the experimental result showing preference for allylic C-H amination product and with the observed trend upon going from catalyst **II** to catalyst **III.** However, the presented computations overestimate the amination:aziridination ratio.

CONCLUSIONS

From above presented results we draw the following conclusions:

1. Catalysts $(H_2O)(Rh_2O_2CH)_4$ (**I**), $(H_2O)(Rh_2(AcO)_4$ (**II**), and $(H_2O)(Rh_2(esp)_2$ (**III**) have a diamagnetic closed shell singlet state with

$[\sigma(d_{zz}+d_{zz})]^2[\pi(d_{xz}+d_{xz})]^2[\pi(d_{yz}+d_{yz})]^2[\sigma(d_{xy}+d_{xy})]^2[\pi^*(d_{xy}-d_{xy})]^2[\pi^*(d_{xz}-d_{xz})]^2[\pi^*(d_{yz}-d_{yz})]^2[\sigma^*(d_{zz}-d_{zz})]^0$ electron configuration. Thus, the Rh-Rh bond in these complexes is formally a single bond and the Rh-centers are in their +2 oxidation states. Their triplet states, with one unpaired spin on each Rh center, lie about 15-17 kcal/mol higher in energy. For all triplet state catalysts, the Rh-Rh bond has slightly larger than half-bond with half σ- and half π-bonds. Therefore, at their triplet state, these complexes have an $[\sigma(d_{zz}+d_{zz})]^2[\pi(d_{xz}+d_{xz})]^2[\pi(d_{yz}+d_{yz})]^2[\sigma(d_{xy}+d_{xy})]^2[\pi^*(d_{xy}-d_{xy})]^2[\pi^*(d_{xz}-d_{xz})]^2[\pi^*(d_{yz}-d_{yz})]^1[\sigma^*(d_{zz}-d_{zz})]^1$ electron configuration.

2. Active species in all cases are the triplet state dirhodium-nitrene complexes with nearly two unpaired spins delocalized between the N-center and Rh-Rh bond. Upon nitrenoid formation, the Rh–Rh single bond of triplet catalyst has partially broken to form Rh-N bond with one σ-bond and two "one-electron π-bonds". In the singlet state, the Rh-N bond of the nitrenoids can be characterized as a double bond (with one σ- and one π-bonds) and N-lone pair. Thermodynamic stability of nitrenoids increases via **I** < **II** < **III** for given substrate.
3. The C-H bond amination in the studied nitrenoids proceeds via triplet-to-singlet surface crossing and singlet concerted C-H insertion transition state ^{X}**I-TS1-s**. The calculated energy barriers correlate with the trend in homolytic bond dissociation energy of the activated C-H bonds.
4. In general, allylic C-H amination is also a concerted C-H insertion process. However, the competing C=C double bond aziridination follows a stepwise pathway involving the formation of an eight-membered cyclic radical intermediate and radical coupling to produce singlet aziridination product.
5. Computed trends in electronic structure and reactivity are consistent across the studied catalysts. However, the computed selectivity is sensitive to the catalyst used in the calculations. Thus, one should be careful about choosing a model based on the properties of interest, especially selectivity.
6. Comparison of the above presented results for catalysts $(H_2O)Rh_2(O_2CH)_4$ (**I**), $(H_2O)Rh_2(AcO)_4$ (**II**) and $(H_2O)Rh_2(esp)_2$ (**III**) with the available (limited) data for the $Rh_2(O_2CH)_4$, $Rh_2(AcO)_4$, and $Rh_2(esp)_2$ catalysts (see [22-24]), show that, in general, presence of axial water molecule does not alter mechanistic outcomes.

ACKNOWLEDGMENT

This work was supported by the National Science Foundation under the CCI Center for Selective C–H Functionalization (CHE-1700982). We gratefully acknowledge NSF MRI-R2 grant (CHE-0958205 for D.G.M.) and the use of the resources of the Cherry Emerson Center for Scientific Computation.

Appendix A. Supplementary data

Supplementary data related to this article can be found at:

It contains: Selected singlet triplet state NBOs of $(H_2O)Rh_2(O_2CH)_4$ catalyst with their electron populations; Selected NBO orbitals of the ^{A}**I0a-s** and ^{A}**I0a-t** nitrene complexes; Selected canonical molecular orbitals of the ^{A}**I0b-t** nitrene complex; Catalytic active nitrenoids relevant for the allylic C-H amination and C=C double bond aziridination. Their

selected geometrical parameters (Å) and spin population values; Catalytic active nitrenoids relevant for primary, secondary, tertiary and benzylic C-H activation in dirhodium-sulfamate systems. Their selected geometrical parameters (Å) and spin population values; Selected geometrical parameters (Å) and spin population analyses of the singlet and triplet state pre-reaction nitrenoids, transition states and products for the primary, secondary, tertiary and benzylic C-H amination by catalyst $(H_2O)Rh_2(O_2CH)_4$ (**I**); Selected geometrical parameters (Å) and spin population analyses of the singlet and triplet state pre-reaction nitrenoids, transition states and products for the allylic C-H amination catalyzed by $(H_2O)Rh_2(O_2CH)_4$ (**I**); Selected geometrical parameters (Å) and spin population analyses of the triplet state pre-reaction nitrenoids, transition states and products for the allylic C-H amination and C=C double bond aziridination catalyzed by $(H_2O)Rh_2(O_2CH)_4$ (**I**); Selected geometrical parameters (Å) and spin population analyses of the singlet and triplet state pre-reaction nitrenoids, transition states and products for the tertiary and benzylic C-H amination catalyzed by $(H_2O)Rh_2(O_2CH)_4$ (**I**), $(H_2O)Rh_2(OAc)_4$ (**II**) and $(H_2O)Rh_2(esp)_2$ (**III**); Selected geometrical parameters (Å) and spin population analyses of the singlet and triplet state pre-reaction nitrenoids, transition states and products for the C=C double bond aziridination catalyzed by $(H_2O)Rh_2(O_2CH)_4$ (**I**), $(H_2O)Rh_2(OAc)_4$ (**II**) and $(H_2O)Rh_2(esp)_2$ (**III**); and some technical comments on the performance of M06L vs. M06 functionals;

Appendix B.
Cartesian Coordinates of all reported structures.

AUTHOR INFORMATION

Corresponding Author

* dmusaev@emory.edu

NOTES

The authors declare no competing financial interests.

REFERENCES

[1] J.A. Halfen, Current Org. Chem. 9 (2005) 657-669.

[2] H.M.L. Davies, M.S. Long, Angew. Chem. Int. Ed. 44 (2005) 3518-3520.

[3] J. Yamaguchi, A.D. Yamaguchi, K. Itami, Angew. Chem. Int. Ed. 51 (2012) 8960-9009.

[4] M.P. Doyle, R. Duffy, M. Ratnikov, L. Zhou, Chem. Rev. 110 (2010) 704-724.

[5] H.M.L. Davies, D. Morton, Chem. Soc. Rev. 40 (2011) 1857-1869.

[6] K. Liao, S. Negretti, D.G. Musaev, J. Bacsa, H.M.L. Davies, Nature, 533 (2016) 230-234.

[7] A. Varela-Alvarez, T. Yang, H. Jennings, K.P. Kornecki, S.N. Macmillan, K.M. Lancaster, J.B.C. Mack, J. Du Bois, J.F. Berry, D.G. Musaev, J. Am. Chem. Soc. 138 (2016) 2327-2341.

[8] (a) K.P.vKornecki, J.F. Berry, Chem. Eur. J. 17 (2011) 5827-5832; (b) J.F. Berry, Dalton Trans. 41 (2012) 700-713; (c) K.P. Kornecki, J.F. Berry, Chem. Comm., 48 (2012) 12097-12099.

[9] (a) S. Toumieux, P. Compain, O.R. Martin, M. Selkti, Org. Lett. 8 (2006) 4493-4496; (b) S. Toumieux, P. Compain, O.R. Martin, J. Org. Chem. 73 (2008) 2155-2162; (c) M. Shen, B.E. Leslie, T.G. Driver, Angew. Chem. Int. Ed. 47 (2008), 5056-5059; (d) J. Wang, B. Stefane, D. Jaber, J.A.I. Smith, C. Vickery, M. Diop, H.O. Sintin, Angew. Chem. Int. Ed. 49 (2010) 3964-3968.

[10] (a) X.–Q. Yu, J.-S. Huang, X.-G. Zhou, C.-M. Che, Org. Lett. 2 (2000) 2233-2236; (b) J.-L. Liang, S.-X. Yuan, J.-S. Huang, C.-M. Che, J. Org. Chem. 69 (2004) 3610-3619; (c) E. Milczek, N. Boudet, S. Blakey, Angew. Chem. Int. Ed. 47 (2008) 6825-6828; (d) W.G. Shon, J. Li, T. Guo, Z. Lin, G. Jia, Organometallics 28 (2009) 6847-6854; (e) S. Fantauzzi, E. Gallo, A. Caselli, F. Ragaini, N. Casati, Chem. Commun. (2009), 3952-3954.

[11] M. Harvey, D.G. Musaev, J. Du Bois, J. Am. Chem. Soc. 133 (2011) 17207-17216.

[12] (a) J.D. Harden, J.V. Ruppel, J.-Y. Gao, X.P. Zhang, Chem. Commun. (2007) 4644-4646; (b) A. Caselli, E. Gallo, S. Fantauzzi, S. Morlacchi, F. Ragaini, S. Cenini, Eur. J. Inorg. Chem. (2008), 3009-3019; (c) H. Lu, V. Subbarayan, J. Tao, X.P. Zhang, Organometallics 29 (2010) 389-393.

[13] (a) F. Avenier, J.-M. Lantour, Chem. Commun. (2004) 1544-1545; (b) Z. Wang, Y. Zhang, H. Fu, Y. Jiang, Y. Zhao, Org. Lett. 10 (2008) 1863-1866; (c) A. Varela-Álvarez, D.G. Musaev, Chem. Sci. 4 (2013) 3758-3764.

[14] (a) P. Brandt, M.J. Södergren, P.G. Anderson, P.-O. Norrby, J. Am. Chem. Soc. 122 (2000) 8013-8020; (b) G. Pelletier, D.A. Powell, Org. Lett. 8 (2006) 6031-6034; (c) M.R. Fructos, S. Trofimrnko, M.M. Diaz-Requejo, P.J. Perez, J. Am. Chem. Soc. 128 (2006) 11784-11791; (d) X. Liu, Y. Zhang, L. Wang, H. Fu, Y. Jiang, Y. Zhao, J. Org. Chem. 73 (2008) 6207-6212; (e) S. Wiese, Y.M. Badiei, R.T. Gephart, S. Mossin, M.S. Varonka, M.M. Melzer, K. Meyer, T.R. Cundari, T.H. Warren, Angew. Chem. Int. Ed. 49 (2010) 8850-8855; (f) S. Guo, B. Qian, Y. Xie, C. Xia, H. Huang, Org. Lett. 13 (2011) 522-525; (g) M. Miyasaka, K. Hirano, T. Satoh, R. Kowalcyk, C. Bolm, M. Miura, M. Org. Lett. 13 (2011) 359-361.

[15] (a) J.-L. Liang, J.-S. Juang, X.-O. Yu, N. Zhu, C.-M. Che, Chem. Eur. J. 8 (2002) 1563-1572; (b) Y. Cui, C. He, J. Am. Chem. Soc. 125 (2003) 16202-16203; (c) Y. Cui, C. He, Angew. Chem. Int. Ed. 43 (2004) 4210-4212; (d) Z. Li, X. Ding, C. He, J. Org. Chem. 71 (2006) 5876-5880; (e) Z. Li, C.R. Rahaman, C. He, Angew. Chem. Int. Ed. 46 (2007) 5184-5186.

[16] (a) F. M. Figg, S. Park, J. Park, S. Chang, D.G. Musaev, Organometallics 33 (2014) 4076–4085; (b) H. Xu, K. Muto, J. Yamaguchi, C. Zhao, K. Itami, D.G. Musaev, J. Am. Chem. Soc. 136 (2014) 14834-14844; (c) K. Muto, J. Yamaguchi, D.G. Musaev, K. Itami, Nature Comm. 6 (2015) 7508.

[17] (a) C. Qin, V. Boyarskikh, J.H. Hansen, K.E. Hardcastle, D.G. Musaev, H.M.L. Davies, J. Am. Chem. Soc. 133 (2011) 19198-19204; (b) H. Wang, D.M. Guptill, A. Varela Alvarez, D.G. Musaev, H.M.L. Davies, Chem. Sci. 4 (2013) 2844-2850; (c) B.D.

McLarney, M.A. Cavitt, T. Donnell, D.G. Musaev, S. France, Chem-A European Journal, 23 (2016) 1129-1135.

[18] C.G. Espino, J. Du Bois, Angew. Chem. Int. Ed. 40 (2001) 598-600.

[19] (a) C.G. Espino, P.M. Wehn, J. Chow, J. Du Bois, J. Am. Chem. Soc. 123 (2001) 6935-6936; (b) K. Guthikonda, J. Du Bois, J. Am. Chem. Soc. 124 (2002) 13672-13673; (c) P.M. Wehn, J. Lee, J. Du Bois, Org. Lett. 5 (2003) 4823-4826; (d) K.W. Fiori, J.J. Fleming, J. Du Bois, Angew. Chem. Int. Ed. 43 (2004) 4349-4352; (e) C.G. Espino, K.W. Fiori, J. Du Bois, J. Am. Chem. Soc. 126 (2004) 15378-15379; (f) K. Guthikonda, P.M. Wehn, B.J. Caliando, J. Du Bois, Tetrahedron 62 (2006) 11331-11342; (g) D.N. Zalatan, J. Du Bois, J. Am. Chem. Soc. 130 (2008) 9220-9221; (h) D.N. Zalatan, J. Du Bois, J. Am. Chem. Soc. 131 (2009) 7558-7559; (j) K.W. Fiori, C.G. Espino, H. Brodsky, J. Du Bois, Tetrahedron 65 (2009) 3042-3051; (i) J. Du Bois, Org. Process Res. Dev. 15 (2011) 758-762; (k) R.H. Perry, T.J. Cahill III, J.L. Roizen, J. Du Bois, R.N. Zare, Proc. Natl. Acad. Sci. USA, 109 (2012) 18295-18299; (l) J. L. Roizen, M.E. Harvey, J. Du Bois, Acc. Chem. Res. 45 (2012) 911-922.

[20] M. Kim, J.V. Mulcaky, C.G. Espino, J. Du Bois, Org. Lett. 8 (2006) 1073-1076.

[21] K.W. Fiori, J. Du Bois, J. Am. Chem. Soc. 129 (2007) 562-568.

[22] X. Zhang, Z. Ke, N.J. DeYonker, H. Xu, Z.-F. Li, X. Xu, X. Zhang, C.-Y. Su, D.L. Phillips, C. Zhao, J. Org. Chem. 78 (2013) 12460-12468.

[23] X. Zhang, H. Xu, C. Zhao, J. Org. Chem. 79 (2014) 9799-9811.

[24] J. Wang, K.C. Zheng, B. Lin, Y. Weng, RSC Advances, 7 (2017) 34783-34794.

[25] (a) Y. Zhao, D.G. Truhlar, J. Chem. Phys. 125 (2006) 194101; (b) Y. Zhao, D.G. Truhlar, Theor. Chem. Acc. 120 (2008) 215-241.

[26] (a) N. Schultz, Y. Zhao, D.G. Truhlar, J. Phys. Chem. A 109 (2005) 4388-4403; (b) N. Schultz, Y. Zhao, D.G. Truhlar, J. Phys. Chem. A 109 (2005) 11127-11143.

[27] W. J. Hehre, L. Radom, P.v.R. Schleyer, J.A. Pople, J. A. Ab initio Molecular Orbital Theory; John Wiley & Sons: New York, 1986.

[28] (a) P.J. Hay, W.R. Wadt, J. Chem. Phys. 82 (1985) 299-310; (b) L.E. Roy, P.J. Hay, R.L. Martin, J. Chem. Theory Comput. 4 (2008) 1029-1031; (c) A.W. Ehlers, M. Bohme, S. Dapprich, A. Gobbi, A. Hollwarth, V. Jonas, K.F. Kohler, R. Stegmann, A. Veldkamp, G. Frenking, Chem. Phys. Lett. 208 (1993) 111-114.

[29] (a) E. Nakamura, N. Yoshikai, M. Yamanaka, J. Am. Chem. Soc. 124 (2002) 7181-7192; (b) E. Nakamura, N. Yashikai, Adv. Synth. Catal. 345 (2003) 2259-1171; (c) D.T. Nowlan, T.M. Gregg, H.M.L. Davies, D.A. Singleton, J. Am. Chem. Soc. 125 (2003) 15902-15911; (d) X. Lin, C. Zhao, C.-M. Che, Z. Ke, D.L. Phillips, *Chem.* Asian J. 2 (2007) 1101-1108; (e) J. Hansen, H.M.L. Davies, J. Org. Chem. 74 (2009) 6555-6563; (f) X. Lin, J. Sun, Y. Xi, B. Pang, Comput. Theor. Chem. 963 (2011) 284-289.

[30] (a) H.T. Bonge, T. Hansen, J. Org. Chem. 75 (2010) 2309-2320; (b) H.T. Bonge, T. Hansen, Tetrahedron Lett. 51 (2010) 5298-5301.

[31] Z. Futera, T. Koval, J. Lezczynski, J. Gu, M. Mitoraj, M. Srebro, J.V. Burda, J. Phys. Chem. A 115 (2011) 784-794.

[32] (a) J. Lloret, J.J. Carbó, C. Bo, A. Lledós, J. Perez-Prieto, Organometallics 27 (2008) 2873-2876; (b) D.L. Lichtenberger, J.R. Pollard, M.A. Lynn, F.A. Cotton, X. Feng, J. Am. Chem. Soc. 122 (2000) 3182-3190.

[33] (a) V. Cadierno, S.E. García-Garrido, J. Gimeno, A. Varela-Álvarez, J.A. Sordo, J. Am. Chem. Soc. 128 (2006) 1360-1370; (b) X. Lin, C.-M. Che, D.L. Phillips, J. Org. Chem. 73 (2008) 529-537; (c) S. Tussupbayev, S.F. Vyboishchikov, Organometallics 27 (2008) 3681-3892; (d) A. Varela-Álvarez, J.A. Sordo, E. Piedra, N. Nebra, V. Cadierno, J. Gimeno, Chem. Eur. J. 17 (2011) 10583-10599; (e) V. Lyaskovskyy, A.I. Olivos Suarez, H. Lu, H. Jiang, X.P. Zhang, B. De Bruin, J. Am. Chem. Soc. 133 (2011) 12264-12273.

[34] M.J. Frisch, G.W. Trucks, H.B. Schlegel, G.E. Scuseria, M.A. Robb, J.R. Cheeseman, G. Scalmani, V. Barone, B. Mennucci, G.A. Petersson, H. Nakatsuji, M. Caricato, X. Li, H.P. Hratchian, A.F. Izmaylov, J. Bloino, G. Zheng, J.L. Sonnenberg, M. Hada, M. Ehara, K. Toyota, R. Fukuda, J. Hasegawa, M. Ishida, T. Nakajima, Y. Honda, O. Kitao, H. Nakai, T. Vreven, J.A. Montgomery, J.E. Peralta, F. Ogliaro, M. Bearpark, J.J. Heyd, E. Brothers, K.N. Kudin, V.N. Staroverov, R. Kobayashi, J. Normand, K. Raghavachari, A. Rendell, J.C. Burant, S.S. Iyengar, J. Tomasi, M. Cossi, N. Rega, J.M. Millam, M. Klene, J.E. Knox, J.B. Cross, V. Bakken, C. Adamo, J. Jaramillo, R. Gomperts, R.E. Stratmann, O. Yazyev, A.J. Austin, R. Cammi, C. Pomelli, J.W. Ochterski, R.L. Martin, K. Morokuma, V.G. Zakrzewski, G.A. Voth, P. Salvador, J.J. Dannenberg, S. Dapprich, A.D. Daniels, O. Farkas, J.B. Foresman, J.V. Ortiz, J. Cioslowski, D.J. Fox, Gaussian 09, Revision B.01, Gaussian, Inc., Wallingford, CT, 2010.

[35] H.T. Chifotides, K.R. Dumbar, In *Multiple Bonds between Metal Atoms*; F.A. Cotton, C.A. Murillo, R.A. Walton, Eds. Springer Science and Business Media, Inc.: New York, 2005.

[36] J. Wolf, R. Poli, J.-H. Xie, J. Nichols, B. Xi, P. Zavalij, M.P. Doyle, Organometallics 27 (2008) 5836-5845.

[37] We are aware that singlet-triplet transitions are forbidden but it is also well-known that such processes take place and even some well-known reactions can only evolve through one of this forbidden surface-crossing.[37] Spin-orbit coupling value for the system considered must be high in order to get an efficient singlet-triplet transition and metallic systems usually satisfy this requirement. Then, throughout the present work we will assume that singlet-triplet surface-crossing processes are fast enough to assure that those electronic states are as populated as their energetics dictate; that is, singlet and triplet states of each intermediate instantly reach their equilibrium population, and kinetic contributions of singlet and triplet states of the transition-state structures only depend on their respective free energy barrier heights.

[38] (a) D.F. McMillen, D.M. Golden, Ann. Rev. Phys. Chem. 33 (1982) 493-352; (b) S.J. Blanksby, G.B. Ellison, Acc. Chem. Res. 36 (2003) 255-263.

[39] (a) D. Feller, J.A. Sordo, J. Chem. Phys. 112 (2000) 5604-5610; (b) D. Feller, J.A. Sordo, J. Chem. Phys. 113 (2000) 485-493; (c) J.A. Sordo, J. Chem. Phys. 114 (2001) 1974-1980; (d) J. Zheng, Y. Zhao, D.G. Truhlar, J. Chem. Theory Comput. 5 (2009) 808-821.